Low-Temperature Flexible Photoanode and Net-Like Pt Counter Electrode for Improving the Performance of Dye-Sensitized Solar Cells

ARTICLE *in* THE JOURNAL OF PHYSICAL CHEMISTRY C · NOVEMBER 2010

Impact Factor: 4.77 · DOI: 10.1021/jp107308r

Low-Temperature Flexible Photoanode and Net-Like Pt Counter Electrode for Improving the Performance of Dye-Sensitized Solar Cells

Lu-Yin Lin,[†] Po-Chin Nien,[†] Chuan-Pei Lee,[†] Keng-Wei Tsai,[†] Min-Hsin Yeh,[†] R. Vittal,[†] and Kuo-Chuan Ho*,[†,‡]

Department of Chemical Engineering and Institute of Polymer Science and Engineering, National Taiwan University, Taipei 10617, Taiwan

Received: August 4, 2010; Revised Manuscript Received: October 18, 2010

Back-illuminated dye-sensitized solar cell (DSSC) based on a flexible TiO_2/Ti foil photoanode and a high transparent platinum counter electrode (Pt-CE) has been developed by using a net-like Pt-CE and a relatively low annealing temperature (120 °C) for the preparation of a binder-free TiO_2 paste. The TiO_2/Ti foil photoanode was annealed at various temperatures (120, 250, 350, and 450 °C). Solar-to-electricity efficiencies (η) of 4.34, 3.72, and 3.40% were obtained for the DSSCs with TiO_2/Ti photoanodes annealed at 350, 250, and 120 °C, respectively, which are comparable to the value of 4.33% obtained at 450 °C. The DSSC with Ti foil as working substrate shows better performance ($\eta = 3.40\%$) than that of a DSSC with indium tin oxide (ITO)/polyethylene naphthalate (PEN) as the substrate (2.08%), both prepared through a low-temperature fabrication process (120 °C). The η is further improved to 4.77% at 350 °C by using a net-like Pt-CE. Explanations are substantiated through scanning electron microscopy (SEM), X-ray diffraction analysis, cyclic voltammetry (CV), electrochemical impedance spectroscopy (EIS), and transmission spectral studies.

1. Introduction

Flexible dye-sensitized solar cells (DSSCs) are convenient portable power sources and can be used in complex environments. Also, roll-to-roll production is possible in this case. For the time being, most of research works have been focused on the fabrication of flexible DSSCs based on nanocrystalline TiO_2 electrodes with plastic working substrates.[1−6] DSSCs with this type of plastic substrates usually show much lower solar-to-electricity efficiency (η) than that of a DSSC with transparent conductive oxide glass as the working electrode; this lower efficiency is the result of poor particle interconnections of TiO_2, prepared at low temperature, which cannot be avoided in the case of plastic substrates. This is the major problem concerning the development of flexible DSSCs with plastic substrates. From this point of view, metal substrates are alternatives for plastic substrates, because of their wider compatibility with a far higher range of annealing temperatures.[7−12] It is anticipated that the application of a metal sheet as the support of TiO_2 in a DSSC not only can reduce the cost of fabrication of the solar cell but also can improve the cell performance, owing to its inherent nature of better conductivity and light scattering nature, as compared to those of a plastic sheet.

If an annealing temperature lower than 450 °C is used, the residual of the binder would become an insulating core to block the transport path of the electrons, thereby reducing the electron-transport rate and electron lifetime.[13] Lewis et al. suggested that incomplete combustion of the organics gives a deposit that reduces cell efficiency at low temperature.[14] Therefore, the incorporation of organic binder in a TiO_2 paste is not appropriate for a low temperature preparation of TiO_2.

Besides, in the case of a metal-based photoanode, the illumination should be done from the back side because of the nontransparent nature of metal substrates. From this standpoint, the Pt counter electrode (Pt-CE) of a flexible cell assumes great importance. In the case of a back-illuminated DSSC, the light utilization by the photoanode is much less than that in the case of a front-illuminated DSSC. In this regard, the preparation of a Pt-CE with high transmittance is significant.

Kang et al. fabricated transparent counter electrodes by chemically reducing Pt^{2+} in $NaBH_4$ solution;[9] Ito and co-workers used electrochemical deposition technique to prepare Pt-CE with high transmittance.[8] Onoda et al. used sputtered Pt as transparent layer on CEs to assemble DSSCs with flexible photoanodes.[15]

In this work, we prepared TiO_2/Ti photoanodes with binder-free TiO_2 paste through a low-temperature annealing process (120−450 °C). We used Ti metal as the substrate for the photoanode and utilized the advantage of annealing up to 350 °C to achieve an efficiency of 4.77% for the pertinent DSSC, which is remarkable for a low-temperature-fabricated DSSC. In order to avoid any insulating core due to the organic binders, we made the TiO_2 without using any such binder.

Necessitated by the back-illumination, a new strategy of using a net-like Pt-CE is introduced in this study, which showed a transmittance considerably higher than that shown by normal Pt-CE and consequently a higher efficiency (η) than that achieved in the case of the DSSC with normal Pt-CE.

2. Experimental Section

Lithium iodide (LiI, synthetical grade) and iodine (I_2, synthetical grade) were obtained from Merk; *N*-methylbenzimidazole (NMBI, 99%), 4-tert-butylpyridine (TBP, 96%), and tert-butyl alcohol (tBA, 96%) were obtained from Acros. Terabutylammonium iodide (TBAI, 98%), titanium tetraisopropoxide (TTIP, >98%), acetonitrile (ACN, 99.99%), acetylacetone (AA, >99.5%), ethanol (99.5%), neutral cleaner, isopropyl

* Corresponding author. Tel: +886-2-2366-0739; Fax: +886-2-2362-3040; E-mail: kcho@ntu.edu.tw.
[†] Department of Chemical Engineering.
[‡] Institute of Polymer Science and Engineering.

10.1021/jp107308r
Published on Web 11/11/2010

SCHEME 1: Mask Patterns with Hole-Widths of (a) 100 μm and (b) 200 μm

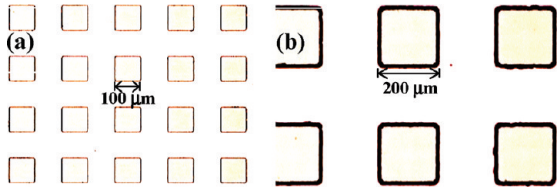

alcohol (IPA, 99.5%), and lithium perchlorate ($LiClO_4$, ≥98.0%) were obtained from Aldrich. 3-Methoxypropionitrile (MPN, 99%) was obtained from Fluka. The positive photoresist, AZP 4620, and the developer, MP450, were purchased from Fujifilm. For the organic solvent electrolyte, a mixture of 0.4 M LiI, 0.04 M I_2, 0.4 M TBAI, and 0.3 M NMBI in MPN/ACN (1:1) was used. Commercial titanium dioxide (P25, Degussa, 1 g) was added into a 6 mL solution of tBA and DI-water (volume ratio of 2:1), and the contents were thoroughly mixed. The mixture was stirred for 5 days, and the binder-free TiO_2 paste was thus obtained. The conducting glass (ITO, 10 Ω/sq.) and Ti foil (0.40 mm, Fuu Cherng Co. Ltd., Taiwan) were first cleaned with a neutral cleaner and then washed with DI-water, acetone, and IPA, sequentially. The surface of the Ti foil was treated with a solution of TTIP (0.028 g) in ethanol (10 mL) in order to make a good mechanical contact between the metal Ti foil and the TiO_2 film. A 10 μm thick film of TiO_2 was then coated on the treated Ti foil through doctor blade technique; a portion of 0.4 × 0.4 cm^2 was selected from the film as the active area by removing the side portions by scrapping. The TiO_2 film was gradually heated to various temperatures (120, 250, 350, and 450 °C) in an oxygen atmosphere and subsequently annealed at each of these temperatures for 30 min. Film thickness was determined by using a surface profilometer (Sloan Dektak 3030). X-ray diffraction patterns (XRD, MO3XHF, MAC) were obtained to note any changes in the Miller indices of Ti foil due to its annealing at different temperatures. Surface morphologies of TiO_2 at various annealing temperatures were observed by scanning electron microscopy (SEM, LEO 1530, LEO Electron Microscopy).

After annealing at one of the above-mentioned temperatures and cooling to 80 °C, the TiO_2/Ti photoanode was immersed in a 3 × 10^{-4} M solution of *cis*-di(thiocyanato)-*N,N′*-bis(2,2′-bipyridyl-4-carboxylicacid-4′-tetrabutyl ammonium carboxylate) ruthenium(II) (N719, Solaronix S.A., Aubonne, Switzerland) in acetonitrile and tert-butyl alcohol (volume ratio of 1:1) at room temperature for 24 h. The net-like Pt-CE (CE-B) was prepared in two designs (CE-B100 and CE-B200), because this type of CE is novel and we had no idea about which one works well. Though the designs are different, as shown in Scheme 1, the method of preparing the CEs is the same. CE-B was prepared as follows. An ITO glass was covered with chemical positive photoresist (AZP 4620) by spin-coating at 3 000 rpm for 30 s and hardened at 90 °C for 90 s on a hot plate. After soft-baking of photoresist-covered ITO glass, a film mask (10 000 dpi) made by Taiwan Kong King Company (Scheme 1) was applied to it. The substrate of the ITO glass was exposed to UV light (12 s, 10 mJ/cm^2) with the film mask, and the exposed photoresist was removed by using a developer soup (MP450:H_2O = 1:4) for 50 s. Two types of mask patterns as shown in Scheme 1 are prepared, one with transparent squares of 100 μm sides and the other with transparent squares of 200 μm sides. Pt layer was deposited on the patterns by sputtering for 5, 10, 15, 25, 30, and 40 s (under sputter current of 40 mA). Unwanted photoresist was removed completely in an acetone solution by using a supersonic method. Pt-CEs without net-like pattern (CE-A) were also prepared. The dye-coated TiO_2 foil was then assembled with a Pt-CE prepared as described already; the two electrodes were separated by a 25 μm thick gasket made of ionomer Surlyn (SX1170-25, Solaronix S.A., Aubonne, Switzerland) and sealed by heating. The electrolyte was injected into the gap between the electrodes by capillarity. For this injection purpose, a hole was previously made in the CE with a drilling machine. After the electrolyte injection, the hole was sealed with hot-melt glue.

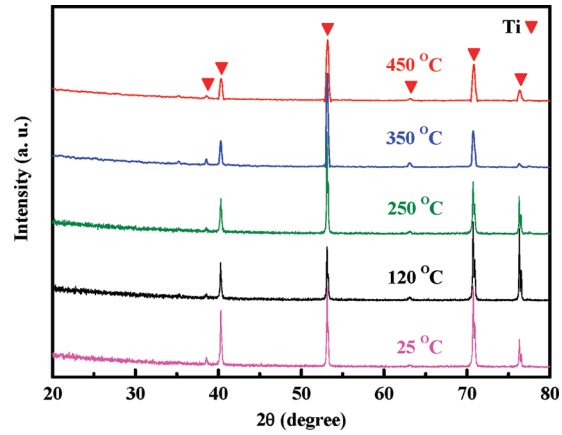

Figure 1. XRD patterns of Ti foils, obtained after annealing them separately at different temperatures.

The DSSC was illuminated by a class A quality solar simulator (PEC-L11, AM1.5G, Peccell Technologies, Inc.) from the side of Pt-CE and the incident light intensity (100 mW/cm^2) was calibrated with a standard Si Cell (PECSI01, Peccell Technologies, Inc.). The photoelectrochemical characteristics of the DSSC were recorded with a potentiostat/galvanostat (PGSTAT 30, Autolab, Eco-Chemie, The Netherlands). UV−vis spectrophotometric data (V-570, Jasco, Japan) and cyclic voltammetry (CV) measurements were used to investigate, respectively, the transmittance properties and the catalytic abilities of the Pt-CEs. The catalytic activities of CE-A, CE-B100, and CE-B200 for the reduction of triiodide ions were assessed by CV, carried out at a scan rate of 50 mV/s by using a three-electrode cell with Pt-coated FTO glass as the working electrode, a Pt foil as the auxiliary electrode, and Ag/Ag^+ electrode as the reference electrode. The electrolyte solution contained 1 mM I_2, 10 mM LiI, and 0.1 M $LiClO_4$ in ACN. Electrochemical impedance spectra (EIS) were obtained by the above-mentioned potentiostat/galvanostat equipped with an FRA2 module under a constant light illumination of 100 mW/cm^2. The frequency range explored was 10 mHz−65 kHz. The applied bias voltage was set at the open-circuit voltage of the DSSC, between the Pt-CE and the dye/TiO_2/Ti photoanode, starting from the short-circuit condition; the corresponding ac amplitude was 10 mV. The impedance spectra were analyzed by using an equivalent circuit mode.[16,17]

3. Results and Discussion

For a metal-based DSSC, the metal oxide formed at the substrate during the annealing process of a TiO_2 photoanode is a hindrance for the transportation of electrons through the substrate. Figure 1 shows XRD patterns of Ti foil annealed at various temperatures. The XRD patterns show consistent intensity changes in all the peaks of Ti metal. With the increase of sintering temperature, the peaks show a decrease, indicating partial formation of TiO_2 from Ti with temperature increase. To avoid the formation of metal oxide from Ti, a low-

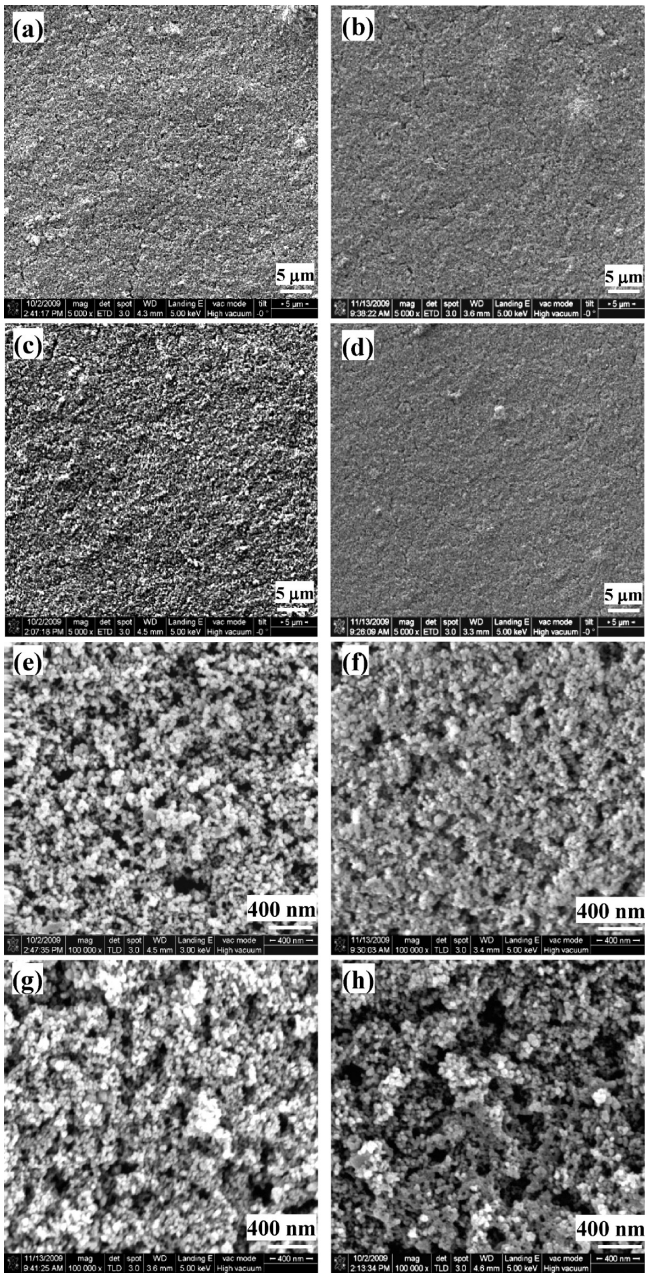

Figure 2. SEM images of TiO_2 films annealed at 120 °C (a, e), 250 °C (b, f), 350 °C (c, g), and 450 °C (d, h); (a−d) low magnification and (e−h) high magnification.

temperature process is required to prepare the photoanode, and at the same time, TiO_2 interparticle connection has to be improved; this may be achieved by using a highly viscous paste without using any polymer binder material, which otherwise would remain as an insulating core in the dried TiO_2 film and would block carrier transport between TiO_2 particles.[3] Figure 2 illustrates the SEM images of TiO_2 film prepared by using a binder-free paste and annealed at 120, 250, 350, and 450 °C. The films are in general mesoporous, uniform, and crack-free, as observed both at low and high magnifications. Careful observation at low magnification however reveals that Figure 2a,b shows compacted particles, whereas Figure 2c,d show distinct and distributed particles with a porosity higher than that observed in the case of films of Figure 2a,b. For the binder-free paste, the interparticle connection of nanocrystalline TiO_2 (necking reaction) is assumed to occur through the dehydration of hydrogen-bonded network of TiO_2 nanoparticles at low

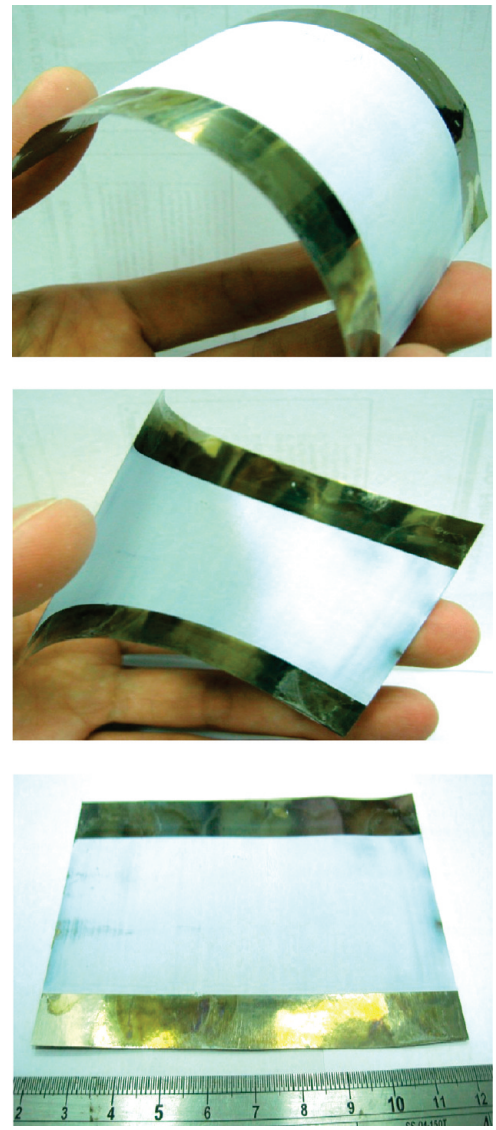

Figure 3. Pictures of large-size flexible TiO_2/Ti photoanodes, annealed at 120 °C. The area of TiO_2 film is 10 × 8 cm^2 in each case. The scale of the ruler in the background is also in centimeter.

temperatures of 120−150 °C, in which the TiO_2 particles were surrounded by water molecules and their surfaces were covered with hydroxyl groups before heating to these temperatures.

To be applicable in various conditions, the endurance of bending is critical for a flexible photoanode. Figure 3 exhibits the flexible TiO_2/Ti photoanode (10 × 5cm^2) under bending condition. The photoanode is exfoliation-free, and its Ti foil is well adhered with crack-free TiO_2 film; these properties show excellent flexibility of the photoanode.

Photovoltaic performance of the DSSCs with TiO_2/Ti photoanodes annealed at 120, 250, 350, and 450 °C are shown in Figure 4a, and the corresponding parameters are listed in Table 1. Efficiencies (η) of 4.34, 3.72%,and 3.40% were obtained for annealing temperatures of 350, 250, and 120 °C, respectively, which were competitive with 4.33% obtained at 450 °C. Table 1 shows that V_{oc} and J_{sc} increase with increasing annealing temperature; this is attributed to better interparticle connection and improved electron transportation. FF shows a decreasing tendency with increasing tempereature; this behavior of FF can be due to increasing resistance in the TiO_2 film owing to the formation of a metal oxide layer at the surface of the Ti substrate at higher annealing temperatures. Figure 4b exhibits the pho-

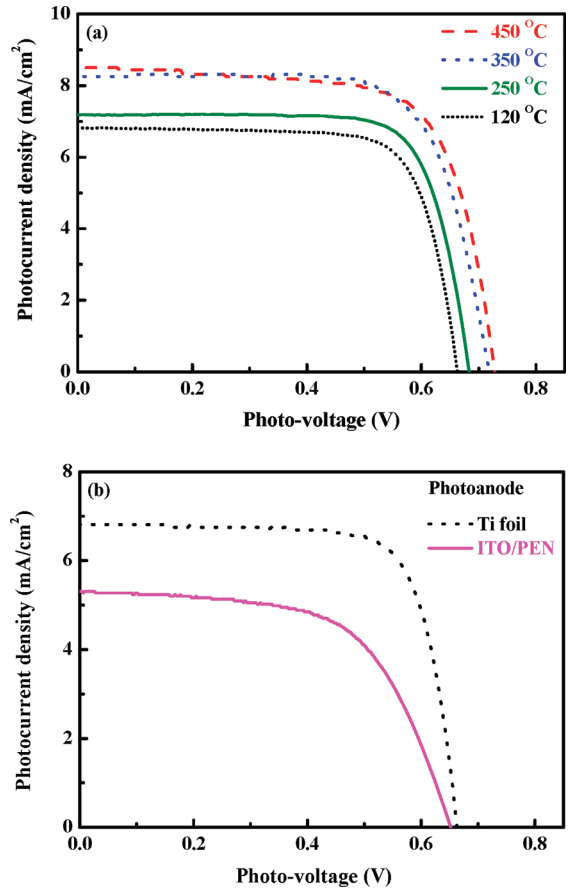

Figure 4. Photocurrent−voltage characteristics of DSSCs with (a) TiO_2/Ti photoanodes annealed at 120, 250, 350, and 450 °C and with (b) TiO_2/Ti and TiO_2/ ITO/PEN photoanodes annealed at 120 °C. The measurements were made at 100 mW/cm^2 light intensity.

TABLE 1: Photovoltaic Parameters of the DSSCs with TiO_2/Ti Photoanodes Annealed at 120, 250, 350, and 450 °C[a]

T (°C)	V_{oc} (V)	J_{sc} (mA/cm^2)	FF	η (%)
450	0.73	8.50	0.70	4.33
350	0.72	8.25	0.73	4.34
250	0.68	7.19	0.75	3.72
120	0.66	6.81	0.75	3.40

[a] 100 mW/cm^2 light intensity was introduced from the CE side.

tovoltaic performance of two DSSCs with binder-free TiO_2 films on Ti foil and ITO/PEN sustrates annealed at 120 °C. Efficiencies (η) of 3.40 and 2.08% were obtained for the DSSCs with Ti foil and ITO/PEN, respectively. The corresponding V_{oc}, J_{sc}, and FF of the DSSC with Ti foil are better than those of the DSSC with ITO/PEN. The enhanced photovoltaic performance in favor of the cell with Ti foil may be attributed to the intrinsic properties of Ti, namely, better scattering surface to utilize the light adequately and better conductivity, compared to those of ITO/PEN.[15,18,19]

Back-illuminated DSSC are plagued with increased optical losses because of reverse lighting; both its CE and its bulk electrolyte shade the photoactive layer from being struck by direct light. In view of this, preparation of a high-transparency Pt-CE is critical for a back-illuminated DSSC.

Figure 5 shows the transmittance of CE-A, CE-B100, and CE-B200, where the net width of CE-B100 is 100 μm and that of CE-B200 is 200 μm; all the CEs were sputtered for 5, 10, 15, 25, 30, and 40 s. Images of CE-B100 and CE-B200, obtained by an optical microscopy, are shown in Figure 6. The transmittance decreases with increasing deposition time of Pt. The transmittance is nearly the same for both CE-B100 and CE-B200 at all the wavelengths; however, is higher than that of

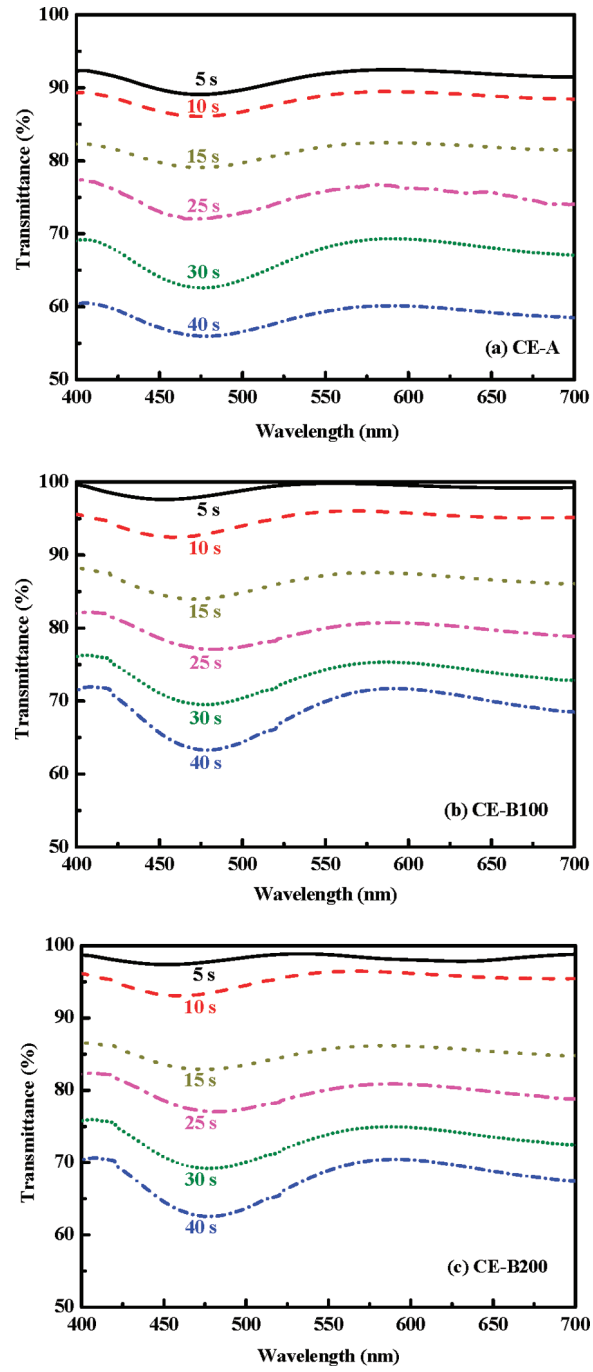

Figure 5. Transmittance spectra of (a) CE-A, (b) CE-B100, and (c) CE-B200 obtained with different deposition times of Pt layers (baseline with bare ITO electrode).

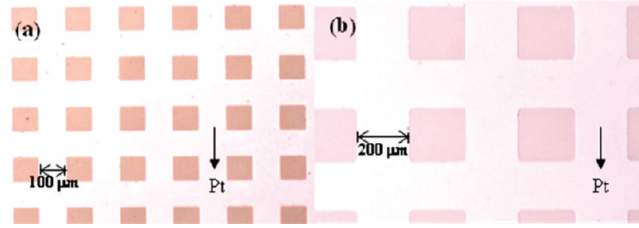

Figure 6. Images of CE-B100 and CE-B200, obtained by an optical microscopy.

TABLE 2: Photovoltaic Parameters of the DSSCs with CE-A for Various Deposition Times, Measured at 100 mW/cm^2 Light Intensity and Illuminated from the CE Side[a]

deposition time (s)	V_{oc} (V)	J_{sc} (mA/cm^2)	FF	η (%)	R_{ct1} (Ω)	R_{ct2} (Ω)
5	0.72	8.25	0.73	4.34	3.02	21.94
10	0.76	7.81	0.73	4.29	2.73	23.82
15	0.75	6.81	0.74	3.78	1.92	37.18
25	0.72	5.83	0.76	3.22	1.85	42.03
30	0.74	5.47	0.71	2.88	1.73	49.74
40	0.73	4.30	0.75	2.35	1.67	66.00

[a] The table also shows the corresponding values of the charge-transfer resistances, R_{ct1} and R_{ct2}.

TABLE 3: Photovoltaic Parameters of the DSSCs with CE-B100 for Various Deposition Times, Measured at 100 mW/cm^2 Light Intensity and Illuminated from the CE Side[a]

deposition time (s)	V_{oc} (V)	J_{sc} (mA/cm^2)	FF	η (%)	R_{ct1} (Ω)	R_{ct2} (Ω)
5	0.74	7.69	0.74	4.19	6.99	25.95
10	0.76	8.69	0.73	4.77	6.75	19.74
15	0.76	7.81	0.73	4.29	6.65	25.66
25	0.74	7.38	0.73	3.99	6.41	30.66
30	0.73	7.00	0.74	3.78	5.32	36.51
40	0.72	6.63	0.74	3.57	4.05	42.05

[a] The table also shows the corresponding values of the charge-transfer resistances, R_{ct1} and R_{ct2}.

TABLE 4: Photovoltaic Parameters of the DSSCs with CE-B200 for Various Deposition Times, Measured at 100 mW/cm^2 Light Intensity and Illuminated from the CE Side[a]

deposition time (s)	V_{oc} (V)	J_{sc} (mA/cm^2)	FF	η (%)	R_{ct1} (Ω)	R_{ct2} (Ω)
5	0.76	7.38	0.72	4.01	9.04	31.53
10	0.74	8.38	0.73	4.52	8.64	21.08
15	0.73	7.50	0.76	4.18	8.51	25.32
25	0.75	6.81	0.75	3.82	8.37	34.53
30	0.76	6.38	0.75	3.40	7.72	38.74
40	0.75	5.60	0.72	3.04	7.39	40.56

[a] The table also shows the corresponding values of the charge-transfer resistances, R_{ct1} and R_{ct2}.

CE-A for all the sputtering periods. It can be noticed that the transmittance of CE-B100 or CE-B200 for the sputtered period of 10 s is higher than that of CE-A for the sputtered period of 5 s; the reason for this is that the sputtered area in the case of CE-B100 or CE-B200 is far less than that of CE-A, owing to the design of CE-B100 and CE-B200.

Tables 2−4 list the photovoltaic parameters of the DSSCs with CE-A, CE-B100, and CE-B200, respectively, for various deposition times. Behaviors of these photovoltaic characteristics as a function of the Pt deposition time for the DSSCs with CE-A, CE-B100, and CE-B200 are shown in Figure 7. In the case of a front-illuminated DSSC, a thickness of the Pt film in the range of 10−415 nm has no significant influence on the performance of the cell.[20] This, however, is not expected to be the case for a back-illuminated DSSC, because transmission of light, the driving force for a DSSC, should be determined by the Pt layer and thus depends on the thickness of this layer. In general, for a Pt deposition time longer than 10 s, the cell performance is better for the DSSCs with CE-B100 and CE-B200, as compared to that of the cell with CE-A; this is due to the higher transmittance of CE-B100 and CE-B200 than that of CE-A, which can enhance the photo-response. The photo-current density and the cell efficiency show a decreasing tendency with increasing deposition time of Pt in all the cases, attributable to the increasing resistance to the light transmittance with increasing thickness of the Pt layer. In the cases of CE-B100 and CE-B200, these two parameters decrease at the deposition period of 5 s, with reference to those at the deposition periods of 10 and 15 s; a too small quantity of Pt as the catalyst in these cases is seen as the reason for this behavior, because the designs of CE-B100 and CE-B200 are expected to allow a smaller quantity of Pt than the plane design of CE-A. The best cell efficiency of 4.77% was obtained for the DSSC with CE-B100 at the Pt deposition time of 10 s; this is clearly due to the higher transmittance of CE-B100 than that of CE-A, because of its special design. Concerning the DSSCs with designed Pt layers, CE-B100 shows better efficiency than CE-B200 at all the deposition periods. Figure 5 indicates that the transmissions of the Pt layers for both CE-B100 and CE-B200 are the same; hence, transmission cannot be the reason for their different performances. Thicknesses of Pt layers in these two cases are assumed to be the same for the same time of their deposition. The third possibility is the electrocatalytic ability of the Pt layers. The surfaces of CEs are not completely covered with Pt owing to the net-like design; the net-like design would cause different diffusion lengths for I_3^- to reach the neighboring Pt particles for the reduction reaction to occur (Scheme 2); thus, the diffusion path for I_3^- is the deciding factor with regard to the performance of cells with these types of net-like Pt as its CEs. The superior cell performance with CE-B100 can be attributed to the shorter diffusion path for I_3^-, compared to that in the case of CE-B200, which has a wider Pt net width of 200 μm. Figure 8 shows overlaid CVs recorded for CE-B100 and CE-B200 with 10 s as deposition periods of the Pt films. The anodic peaks in the figure are denoted by I and II, and the primes indicate the respective cathodic peaks. In an anodic sweep, iodine is oxidized sequentially to triiodide (peak I) and then to iodine (peak II) according to reactions 1 and 2, respectively.

$$3I^- - 2e^- \leftrightarrow I_3^- \quad (1)$$

$$2I_3^- - 2e^- \leftrightarrow 3I_2 \quad (2)$$

When the potential scan is reversed, iodine is reduced first to triiodide (peak II′), then to iodide (peak I′) according to the reactions 3 and 4, respectively,

$$3I_2 + 2e^- \leftrightarrow 2I_3^- \quad (3)$$

$$I_3^- + 2e^- \leftrightarrow 3I^- \quad (4)$$

The absolute cathodic peak currents (I_{pc}) represent the electrochemical activities of Pt-CEs.[21] The absolute I_{pc} in the CVs show higher values for CE-B100, which suggests that the catalytic ability of the Pt layer for I_3^- reduction is better with smaller net width (CE-B100). Figure 8 clearly reveals larger anodic and cathodic peaks and associated charges for CE-B100 than those for CE-B200, except at peak II′, indicating an enhanced reduction capability of CE-B100 for I_3^- ions and the associated enhanced oxidation of I^- ions at the working electrode.

In order to study the charge-transfer resistances at the interfaces, EIS technique was used. Figure 9 shows the EIS data

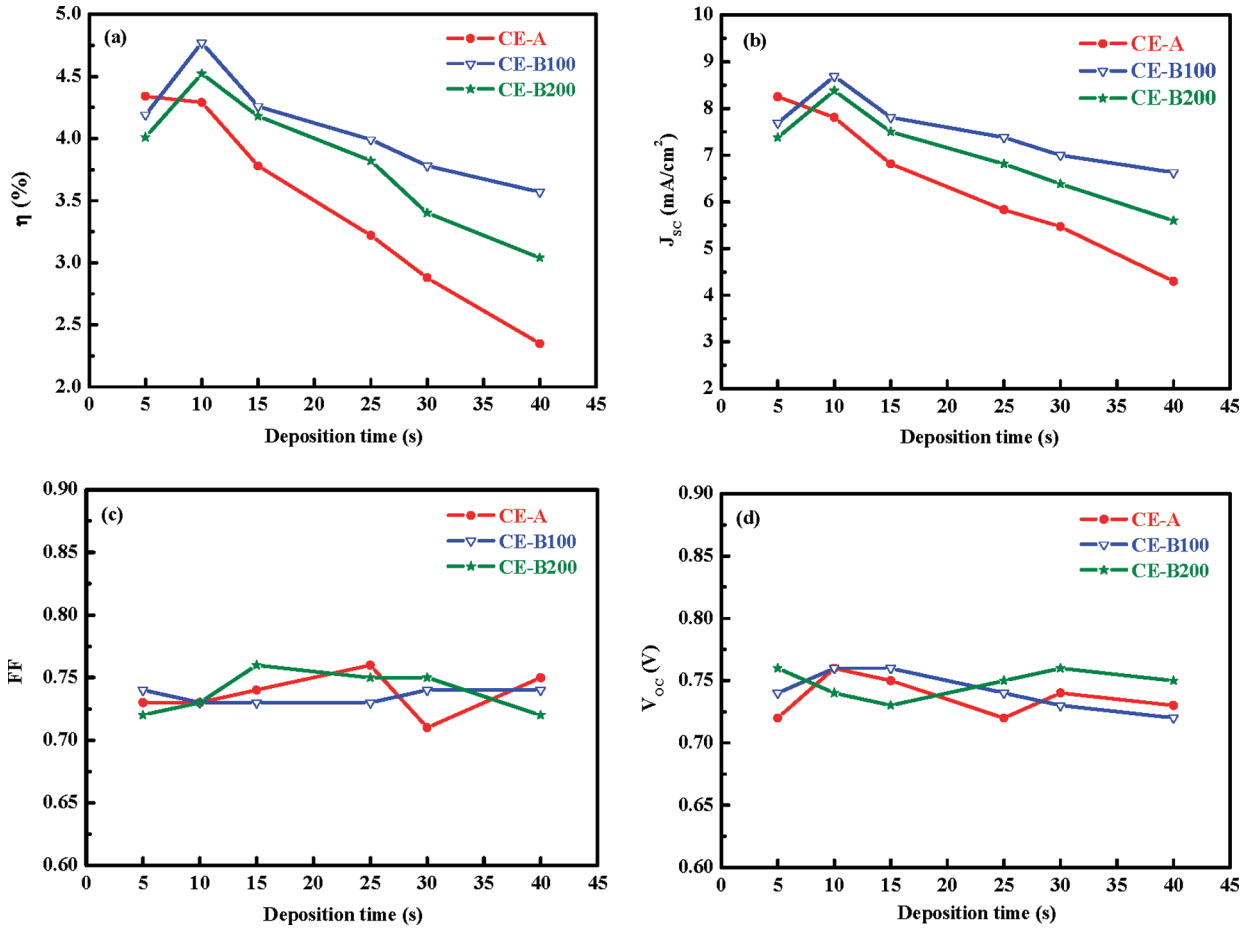

Figure 7. Behaviors of η, J_{sc}, FF, and V_{oc}, each as a function of the Pt deposition time for the DSSCs with CE-A, CE-B100, and CE-B200.

SCHEME 2: Schematic Representation of Different Diffusion Lengths for I_3^- to the Neighboring Pt Particles

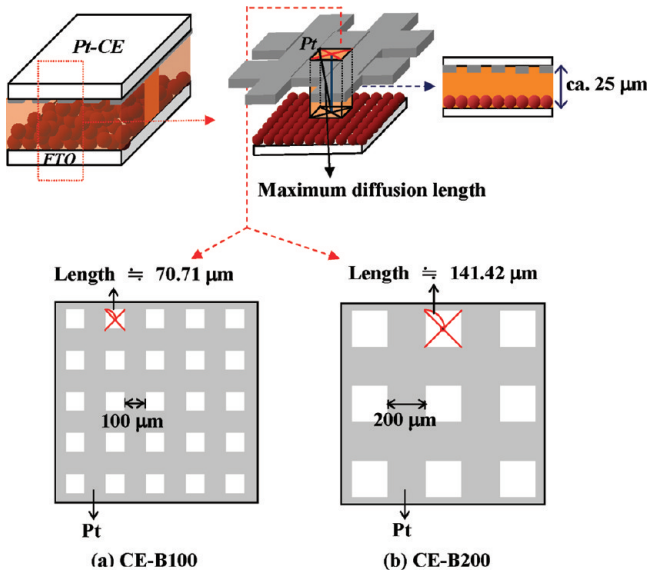

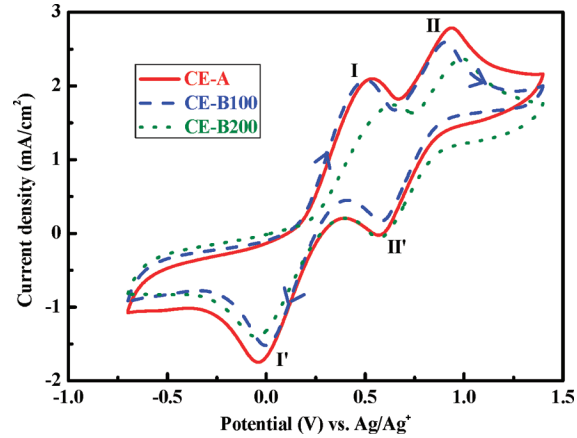

Figure 8. Cyclic voltammograms of CE-A, CE-B100, and CE-B200 with 10 s of deposition time of Pt, in an acetonitrile solution with 10 mM LiI, 1 mM I_2, and 0.1 M $LiClO_4$.

of DSSCs with CE-A, CE-B100, and CE-B200 at various deposition times of their Pt layers; the corresponding values of R_{ct1} and R_{ct2} are listed in Tables 2−4. The equivalent circuit used to analyze the spectra is shown in the inset of Figure 9. In general, impedance spectra of a DSSC show three semicircles in the frequency range of 10 mHz to 65 kHz. The ohmic serial resistance (R_s) corresponds to the overall series resistance. The first and second semicircles from the left correspond to the charge-transfer resistances at the counter electrode (R_{ct1}) and at the TiO_2/dye/electrolyte interface (R_{ct2}), respectively; the third semicircle corresponds to the Warburg diffusion process of I^-/I_3^- in the electrolyte (R_{diff}). In our case, R_{diff} is not obvious, and it is overlapped by R_{ct2}; this is because R_{diff} is negligible in our case because we used very thin spacer (25 μm) and low viscous solvents for the electrolyte (ACN:MPN = 1:1 and the viscosities of ACN and MPN are 0.37 and 1.60 cP, respectively.). Tables 24 show that the values of R_{ct1} decrease steadily with increasing Pt deposition time; this is probably due to a larger surface area available for the catalytic reduction of I_3^- with longer periods of deposition. For DSSCs with CE-A, the

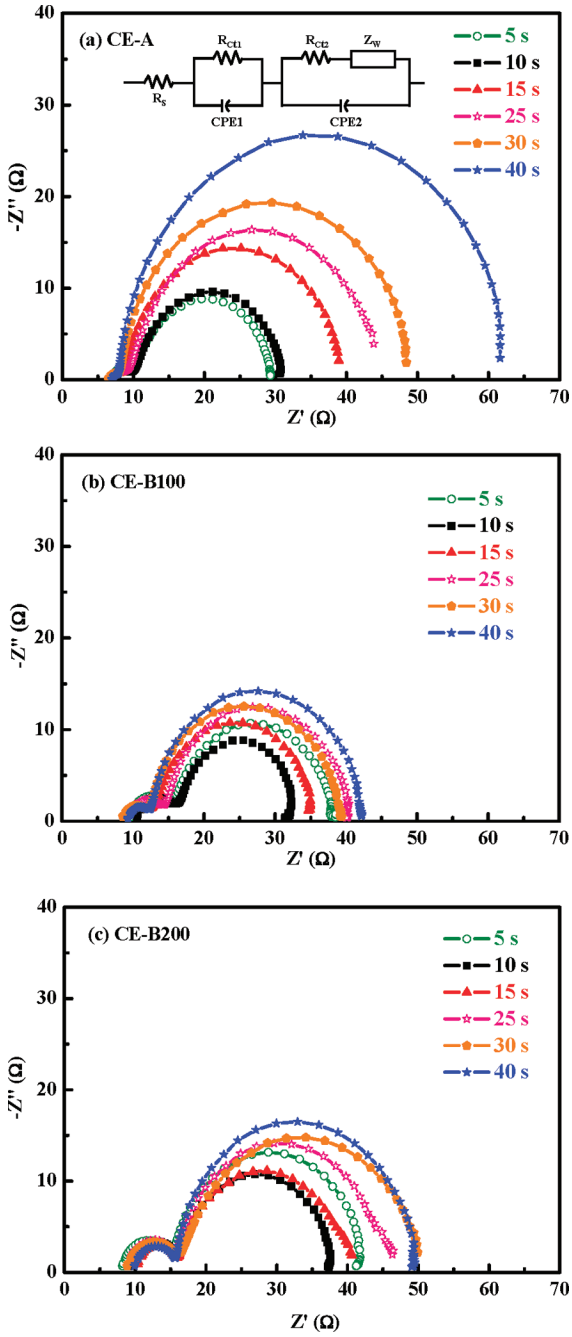

Figure 9. EIS spectra of DSSCs with (a) CE-A, (b) CE-B100, and (c) CE-B200 at various deposition times of their Pt layers and measured at 100 mW/cm^2 light intensity.

R_{ct1} values are remarkably smaller than those observed in the case of DSSCs with CE-B100 and CE-B200, because the Pt layer of CE-A is unbroken and therefore can catalyze the reduction of I_3^- more efficiently than the Pt layers of CE-B100 and CE-B200, which are broken as per their design. This is also evidenced in Figure 8, where the CV of CE-A shows higher currents and charges at all four peaks than those observed for CE-B100 and CE-B200. On the other hand, the values of R_{ct2} show a decreasing tendency with decreasing Pt deposition time for all the DSSCs in this study; this can be explained on the basis of the higher transmittance of Pt layers deposited at shorter periods of time, which would facilitate the excitation of a larger number of dye molecules and thereby would increase the corresponding J_{sc} as is clear from Tables 2−4. Exceptions to these tendencies are noticed in the cases of CE-B100 and CE-B200, where the value of R_{ct2} increases when the deposition time is 5 s; this is a reversal to the tendency discussed above. This exception is probably due to insufficient availability of Pt to catalyze I_3^- reduction; the effect of higher transmittance is probably dominated by the effect of reduced catalysis in these two cases. DSSCs with CE-A show larger values of R_{ct2} compared to those of DSSCs with CE-B100 and CE-B200, at all the deposition times from 10 to 40 s, because a CE-A has lower transmittance than a CE-B100 and a CE-B200 for the same sputter time. These R_{ct2} values are consistent with the corresponding values of J_{sc} (Figure 7b).

In this research, we have focused on net-like Pt-CE. The cells were sintered at low temperatures, which essentially caused low cell efficiencies. The idea of net-like Pt-CE can be useful to other groups of researchers with better skills in cell fabrication to attain higher efficiencies.

4. Conclusions

Flexible TiO_2/Ti photoanode and two types of highly transparent Pt CEs were used to prepare two different DSSCs. A solar-to-electricity conversion efficiency of 4.34% was obtained for a DSSC with binder-free TiO_2 paste prepared at 350 °C, which is virtually the same value of efficiency as that for the cell the TiO_2 of which was prepared at 450 °C. The DSSC with Ti foil as working substrate shows better performance ($\eta = 3.40\%$) than a DSSC with indium tin oxide (ITO)/polyethylene naphthalate (PEN) as the substrate (2.08%), both prepared through a low-temperature fabrication process (120 °C). The DSSCs with net-like Pt-CE (CE-B100 and CE-B200) show better performance than a cell with conventional sputtered-Pt CE (CE-A), essentially owing to better transmittance in the former case. The transmittances for CE-B100 and CE-B200 were found to be higher than those of CE-A, at all the deposition periods, because of the net-like Pt designs in the former two cases. A cell efficiency of 4.77% was achieved with CE-B100 sputtered for 10 s, which is one of the best for a back-illuminated, binder-free DSSC with a flexible photoanode. A new concept of net-like Pt-CE is introduced in this study.

Acknowledgment. This work was supported in part by the National Research Council of Taiwan, Republic of China, under Grants NSC 96-2120-M-002-016 and NSC 97-2120-M-002-012. Some of the instruments used in this study were made available through the financial support of the Academia Sinica, Taipei, Taiwan, Republic of China, under Grant AS-97-TP-A08.

References and Notes

(1) Pichot, F.; Pitts, J. R.; Gregg, B. A. *Langmuir* **2000**, *16*, 5626–5630.
(2) Kijitori, Y.; Ikegami, M.; Miyasaka, T. *Chem. Lett.* **2007**, *36*, 190–191.
(3) Miyasaka, T.; Ikegami, M.; Kijitori, Y. *J. Electrochem. Soc.* **2007**, *154*, A455–A461.
(4) Yamaguchi, T.; Tobe, N.; Matsumoto, D.; Arakawa, H. *Chem. Commun.* **2007**, 4767–4769.
(5) Lee, K. M.; Hu, C. W.; Chen, H. W.; Ho, K. C. *Sol. Energy Mater. Sol. Cells* **2008**, *92*, 1628–1633.
(6) Weerasinghe, H. C.; Sirimanne, P. M.; Simon, G. P.; Cheng, Y. B. *J. Photochem. Photobiol., A* **2009**, *206*, 64–70.
(7) Man, G. K.; Park, N. G.; Kwang, S. R.; Soon, H. C.; Kim, K. J. *Chem. Lett.* **2005**, *34*, 804–805.
(8) Ito, S.; Ha, N. L. C.; Rothenberger, G.; Liska, P.; Comte, P.; Zakeeruddin, S. M.; Péchy, P.; Nazeeruddin, M. K.; Grätzel, M. *Chem. Commun.* **2006**, 4004–4006.
(9) Kang, M. G.; Park, N. G.; Ryu, K. S.; Chang, S. H.; Kim, K. J. *Sol. Energy Mater. Sol. Cells* **2006**, *90*, 574–581.
(10) Jun, Y.; Kim, J.; Kang, M. G. *Sol. Energy Mater. Sol. Cells* **2007**, *91*, 779–784.

(11) Yun, H. G.; Jun, Y.; Kim, J.; Bae, B. S.; Kang, M. G. *Appl. Phys. Lett.* **2008**, 93.

(12) Tan, W.; Yin, X.; Zhou, X.; Zhang, J.; Xiao, X.; Lin, Y. *Electrochim. Acta* **2009**, *54*, 4467–4472.

(13) Longo, C.; Nogueira, A. F.; De Paoli, M. A.; Cachet, H. *J. Phys. Chem. B* **2002**, *106*, 5925–5930.

(14) Lewis, L. N.; Spivack, J. L.; Gasaway, S.; Williams, E. D.; Gui, J. Y.; Manivannan, V.; Siclovan, O. P. *Sol. Energy Mater. Sol. Cells* **2006**, *90*, 1041–1051.

(15) Onoda, K.; Ngamsinlapasathian, S.; Fujieda, T.; Yoshikawa, S. *Sol. Energy Mater. Sol. Cells* **2007**, *91*, 1176–1181.

(16) Han, L.; Koide, N.; Chiba, Y.; Mitate, T. *Appl. Phys. Lett.* **2004**, *84*, 2433–2435.

(17) Han, L.; Koide, N.; Chiba, Y.; Islam, A.; Mitate, T. *Comptes Rendus Chimie* **2006**, *9*, 645–651.

(18) Fang, X.; Ma, T.; Akiyama, M.; Guan, G.; Tsunematsu, S.; Abe, E. *Thin Solid Films* **2005**, *472*, 242–245.

(19) Ma, T.; Fang, X.; Akiyama, M.; Inoue, K.; Noma, H.; Abe, E. *J. Electroanal. Chem.* **2004**, *574*, 77–83.

(20) Fang, X.; Ma, T.; Guan, G.; Akiyama, M.; Kida, T.; Abe, E. *J. Electroanal. Chem.* **2004**, *570*, 257–263.

(21) Kubo, W.; Kambe, S.; Nakade, S.; Kitamura, T.; Hanabusa, K.; Wada, Y.; Yanagida, S. *J. Phys. Chem. B* **2003**, *107*, 4374–4381.

JP107308R